Numerical solution of time-dependent Maxwell's equations for modeling scattered electromagnetic wave's propagation

Adérito Araújo[1], Sílvia Barbeiro[1], Luís Pinto[1], Francisco Caramelo[2], António L. Correia[2], Miguel Morgado[2,5], Pedro Serranho[2,4], Ana Sílvia F. C. Silva[5] and Rui Bernardes[2,3]

[1] *CMUC, Department of Mathematics, University of Coimbra, Portugal*

[2] *IBILI, Faculty of Medicine, University of Coimbra, Portugal*

[3] *ABILI, Coimbra, Portugal*

[4] *Mathematics Section, Department of Science and Technology, Open University, Portugal*

[5] *Department of Physics, Faculty of Science and Technology, University of Coimbra, Portugal*

emails: `alma@mat.uc.pt`, `silvia@mat.uc.pt`, `luisp@mat.uc.pt`,
`fcaramelo@fmed.uc.pt`, `acorreia@aibili.pt`, `mmorgado@ibili.uc.pt`,
`Pedro.Serranho@uab.pt`, `anascsilva@gmail.com`, `rmbernardes@fmed.uc.pt`

Abstract

We present the discontinuous Galerkin method combined with a low-storage Runge-Kutta method as an accurate and efficient way to numerically solve the time-dependent Maxwell's equations. We investigate the numerical scheme in the context of modeling scattered electromagnetic wave's propagation through human eye's structures.

Key words: Maxwell's equations, discontinuous Galerkin method, low-storage Runge-Kutta method, anisotropic permittivity tensor

1 Introduction

The human retina is a complex structure in the eye that is responsible for the sense of vision. It is part of the central nervous system, constituted by layers of neurons interconnected through synapses [7]. There are ten layers in total; one of them is constituted by

photosensitive neurons. There are a number of eye-related pathologies that can be identified by analysis of these retinal layers in detail [7]. All these pathologies can be diagnosed more conclusively with the help of the increasingly popular optical imaging technique – optical coherence tomography (OCT) [3], [15]. In fact, previous studies have established a link between changes in the blood-retina barrier and in optical properties of the retina [1], [2] which can be identified by this exam.

Physically, OCT it is based in low coherence interferometry. This technique uses an electromagnetic wave with a low coherence length. In order to better understand the information carried in an optical coherence tomography, it is crucial to study in detail the behaviour of the electromagnetic wave as it travels through the sample. Several different models have been developed to describe the interactions of the electromagnetic field with biological structures. The first models were based on single-scattering theory [14], which is restricted to superficial layers of highly scattering tissue in which only single scattering occurs. Simulating the full complexity of the retina, in particular the variation of the size and shape of each structure, distance between them and the respective refractive indexes, requires a more rigorous approach that can be achieved by solving Maxwell's equations.

In this work we discuss the numerical discretization of the time-dependent Maxwell's equations. We use the discontinuous Galerkin (DG) method for the integration in space and a low-storage Runge-Kutta method for the integration in time. In the model we consider anisotropic permittivity tensors which arise naturally in our application of interest. We illustrate the performance of the method with some numerical experiments.

2 Maxwell's Equations

We shall consider the time domain Maxwell's equations in the two-dimensional transverse electric (TE) mode. For this case, and assuming no conductivity effects, the equations in the non-dimensional form are

$$\epsilon \frac{\partial E^x}{\partial t} = \frac{\partial H^z}{\partial y} \tag{1}$$

$$\epsilon \frac{\partial E^y}{\partial t} = -\frac{\partial H^z}{\partial x} \tag{2}$$

$$\mu \frac{\partial H^z}{\partial t} = -\frac{\partial E^y}{\partial x} + \frac{\partial E^x}{\partial y}, \qquad \text{in } \Omega \times (0, T], \tag{3}$$

where $E = (E^x, E^y)$ and H^z represent the electric and magnetic fields, respectively, ϵ represents the relative permittivity of the medium and μ is the permeability of the medium and Ω is a two-dimensional domain. The nondimensionalized variables in (1)-(3) are related to the physical variables in the following way

$$\frac{\tilde{x}}{L} = x, \quad \frac{\tilde{y}}{L} = y, \quad \frac{c\tilde{t}}{L} = t, \quad E = Z_0^{-1} E, \quad H^z = H^z,$$

where L is a reference length, c is the speed of light in free space, and $Z_0 = \sqrt{\mu_0/\epsilon_0}$ is the free-space impedance. The set of equations (1)-(3) must be complemented by proper boundary conditions, for instance, the perfect electric boundary condition (PEC) [5]

$$\eta \times E = 0, \qquad \text{on } \partial\Omega, \tag{4}$$

or the Silver-Müller absorbing boundary condition [9]

$$\eta \times E = \sqrt{\frac{\mu}{\epsilon}} \eta \times (H^z \times \eta), \qquad \text{on } \partial\Omega. \tag{5}$$

In both cases η denotes the unit outward normal. To complete the model, initial conditions

$$E_0 = E(0) \quad \text{and} \quad H_0 = H(0), \qquad \text{in } \Omega,$$

must also be considered.

3 The scattered-field formulation

For the investigation of scattering problems in linear materials, we exploit the linearity of the Maxwell's equations (1)-(3) and separate the fields (E, H) into incident (E^i, H^i) and scattered components (E^s, H^s), i.e.,

$$E = E^s + E^i \qquad \text{and} \qquad H = H^s + H^i. \tag{6}$$

Assuming that the incident field is also a solution of the Maxwell's equations we obtain, after some manipulation the scattered field formulation as in [16],

$$\epsilon \frac{\partial E^{x,s}}{\partial t} = \frac{\partial H^{z,s}}{\partial y} + P \tag{7}$$

$$\epsilon \frac{\partial E^{y,s}}{\partial t} = -\frac{\partial H^{z,s}}{\partial x} + Q \tag{8}$$

$$\mu \frac{\partial H^{z,s}}{\partial t} = -\frac{\partial E^{y,s}}{\partial x} + \frac{\partial E^{x,s}}{\partial y} + R, \qquad \text{in } \Omega \times (0, T] \tag{9}$$

with the source terms

$$P(x, y, t) = (\epsilon^i - \epsilon) \frac{\partial E^{x,i}}{\partial t},$$

$$Q(x, y, t) = (\epsilon^i - \epsilon) \frac{\partial E^{y,i}}{\partial t},$$

$$R(x, y, t) = (\mu^i - \mu) \frac{\partial H^{z,i}}{\partial t},$$

where ϵ^i and μ^i represent the relative permittivity and permeability of the medium in which the incident field propagates. In our research, for simplicity, we adopt the pure scattered field formalism in opposition to the total field/scattered field formalism [16].

4 Numerical method

The DG method was first introduced in [11]. In particular, the nodal formulation described in [6] has gained notorious popularity in recent years and it has been extensively used in electromagnetic problems since the first application of the method to Maxwell's equations in 2002 (see [5]). This is the method that we have chosen to use. In opposition to the traditional finite difference (FD) time domain methods [16] based on the Yee's scheme [17] the DG method is a high-order accurate method that can easily handle complex geometries. Moreover, local refinement strategies can easily be incorporate due to the ability of the method to deal with irregular meshes with hanging nodes and local spaces of different orders. When compared to finite element methods [12], the DG method presents the advantages of avoiding the solution of linear systems when explicit time integrators are employed and the suitability for parallel implementation on modern multi-graphics processing units (GPUs) [6].

As starting point of our work we use the MatLab codes for the DG method [6]. The software includes many attributes that we intent to exploit in future work such as three-dimensional routines and nonconforming triangulations. For now, we are concerned with two-dimensional problems and we have restricted our attention to conform triangular elements. Our main focus has been on the implementation of additional features needed for the kind of problems which are in our objectives. For instance, the retinal nerve fiber layer of the retina is a birefringent medium, meaning that tensorial permittivity ϵ needs to be taken into account. We addressed this issue using the numerical scheme presented in [8]. The procedure, based on the so called upwind flux, is fairly simple and can be easily incorporated in the algorithm. Nevertheless, it seems to be efficient and robust for a wide range of problems, since the two by two matrix that represents the tensor ϵ only needs to be invertible. In [8] the authors claim that the method, which is an extension of the basic two-dimensional formulation for isotropic materials to allow anisotropic permittivity tensors, retains the convergence characteristics of the original method. The validation tests that we present in the next section corroborate those findings.

Another aspect of our study concerns the integration in time. The time integration scheme used in the original algorithm [6] is a fourth order, five stage low-storage Runge-Kutta (LSRK) method. Such type of schemes are very popular in this context as they retain the qualities of the original Runge-Kutta schemes while decreasing the memory consumption significatively. However, we recall that explicit methods like the LSRK scheme are subject to the CFL stability condition. In practice, this means that the time step size is proportional to the smallest elements of the spatial mesh [6]. For some problems this condition can have a strong impact on the efficiency of the algorithm. In the future we intent to deal with this issue using local time-stepping strategies [6] or locally implicit time-schemes [4]. For now, we mitigate this restriction implementing the improved fourth order, 14-stage LSRK presented in [10]. With this scheme the authors report a speed improvement of about $40\% - 50\%$ in

relation to the previous fourth order, five stage LSRK method. This gain is consequence of an improved stability region possible by a suitable choice of the coefficients of the scheme. This is a very attractive approach, with very few changes in the code and no additional cost in memory or accuracy. The validation tests that we present in the next section indicate that these conclusions are also valid for the tensorial case.

An important aspect in computational electromagnetic problems is the implementation of absorbing boundary conditions. In our work we have implemented the Silver-Müller boundary condition (5) and the well established and more effective uniaxial perfectly matched layer (UPML) [13]. The UPML can be incorporated in the DG method without any major modification and so far has shown to be an efficient approach.

5   Numerical results

We consider initial conditions, boundary conditions and functions $P(t)$, $Q(t)$ and $R(t)$, such that the system of equations (7)-(9) has the solution

$$E^x = t^2(-\cos(\pi x) - 1)(\frac{1}{3}y^3 - y) \tag{10}$$

$$E^y = 0 \tag{11}$$

$$H^z = \frac{1}{3}t^3(-\cos(\pi x) - 1)(y^2 - 1) \tag{12}$$

with $\epsilon = 4x_c^2 + y_c^2 + 1$, for the results in Tables 1 and 2, and

$$\epsilon = \left[\begin{array}{cc} 4x_c^2 + y_c^2 + 1 & |x_c + y_c| \\ |x_c + y_c| & x_c^2 + 2 \end{array} \right]. \tag{13}$$

for the results in Tables 3-6. In both cases we set $\mu = 1$, $\Omega = [-1, 1]^2$ and $T = 5$. By x_c and y_c we represent the centroid of the triangles. Note that in the implementation ϵ must be constant in each triangle.

h_{max}	$\|E^x - E_h^x\|_{L^2}$	Rate	$\|E^y - E_h^y\|_{L^2}$	Rate	$\|H^z - H_h^z\|_{L^2}$	Rate
1.4142e-01	4.1644e-01	2.0580	4.1702e-01	2.0068	3.5908e-01	2.0297
7.0711e-02	2.4017e-02	2.0265	2.5820e-02	2.0002	2.1537e-02	2.0101
3.5355e-02	1.4469e-03	-	1.6133e-03	-	1.3273e-03	-

Table 1: Convergence rate in the L^2 norm for polynomial approximation of order 1.

From the analysis of Tables 1-4 we observe that the tensorial scheme preserves the optimal rate of convergence of the upwind flux in the scalar case $O(h^{N+1})$, where N denotes the order of the polynomial involved in the approximation. Note also that the order of the

h_{max}	$\|E^x - E_h^x\|_{L^2}$	Rate	$\|E^y - E_h^y\|_{L^2}$	Rate	$\|H^z - H_h^z\|_{L^2}$	Rate
1.4142e-01	8.6363e-04	3.0268	1.0196e-03	3.0124	1.7076e-03	2.9941
7.0711e-02	1.3002e-05	3.0120	1.5660e-05	3.0070	2.6901e-05	2.9978
3.5355e-02	1.9981e-07	-	2.4231e-07	-	4.2159e-07	-

Table 2: Convergence rate in the L^2 norm for polynomial approximation of order 2.

h_{max}	$\|E^x - E_h^x\|_{L^2}$	Rate	$\|E^y - E_h^y\|_{L^2}$	Rate	$\|H^z - H_h^z\|_{L^2}$	Rate
1.4142e-01	5.4515e-01	2.0461	6.2046e-01	1.9949	3.9240e-01	2.0202
7.0711e-02	3.1963e-02	2.0197	3.9055e-02	1.9964	2.3847e-02	2.0067
3.5355e-02	1.9438e-03	-	2.4532e-03	-	1.4767e-03	-

Table 3: Convergence rate in the L^2 norm for polynomial approximation of order 1.

h_{max}	$\|E^x - E_h^x\|_{L^2}$	Rate	$\|E^y - E_h^y\|_{L^2}$	Rate	$\|H^z - H_h^z\|_{L^2}$	Rate
1.4142e-01	8.1456e-04	2.9993	9.4071e-04	3.0184	1.7020e-03	2.9940
7.0711e-02	1.2739e-05	2.9996	1.4328e-05	3.0091	2.6817e-05	2.9979
3.5355e-02	1.9916e-07	-	2.2106e-07	-	4.2022e-07	-

Table 4: Convergence rate in the L^2 norm for polynomial approximation of order 2.

	h_{max}	$\|E_x - E_x^h\|_{L^2}$	Time
original fourth order, 5-stage LSRK	7.0711e-02	3.1963e-02	69.25s
improved fourth order, 14-stage LSRK	7.0711e-02	3.1963e-02	38.35s (44%)
original fourth order, 5-stage LSRK	3.5355e-02	1.9438e-03	514.26s
improved fourth order, 14-stage LSRK	3.5355e-02	1.9438e-03	295.99s (42%)

Table 5: Comparison of the two LSTR methods for polynomial approximation of order 1.

	h_{max}	$\|E_x - E_x^h\|_{L^2}$	Time
original fourth order, 5-stage LSRK	7.0711e-02	1.2739e-05	132.43s
improved fourth order, 14-stage LSRK	7.0711e-02	1.2739e-05	79.71s (39%)
original fourth order, 5-stage LSRK	3.5355e-02	1.9916e-07	1259.94s
improved fourth order, 14-stage LSRK	3.5355e-02	1.9916e-07	745.40s (40%)

Table 6: Comparison of the two LSTR methods for polynomial approximation of order 2.

errors is about the same when we compare the problem with tensorial permittivity and the problem with scalar permittivity.

In Tables 5 and 6 we compare the two different implementations for the time integration. The error is exactly the same for both methods and the running time decreases about 40%.

Even though we only show the results for Ex, in our experiments we found that the error of the other field components, E^y and H^z, present the same type of behaviour.

To illustrate the advantages of the DG method over the FD method we examine the scattering by a dielectric cylinder with a relative permittivity of $\epsilon = 5$. This scatterer with radius $r = 0.5$ and centered at the origin is excited by a Gaussian plane wave propagating along the y direction. We measured the magnetic filed H^z at the point $(x, y) = (-1, 0)$. In Figure 1 we compare the results obtained with both methods. The DG solution was obtained using third-order polynomials and a local refined mesh formed by 920 triangles. This means that the number of unknowns is 9.2×10^3. The FD solution was obtained using a uniform mesh with $h = 1.25 \times 10^{-2}$ implying 4.0×10^4 unknowns. Our experiments show that the DG method is more accurate and efficient. The error, in the Euclidean norm, is 1.5827×10^{-1} for the DG method and 3.6668×10^{-1} for the FD method.
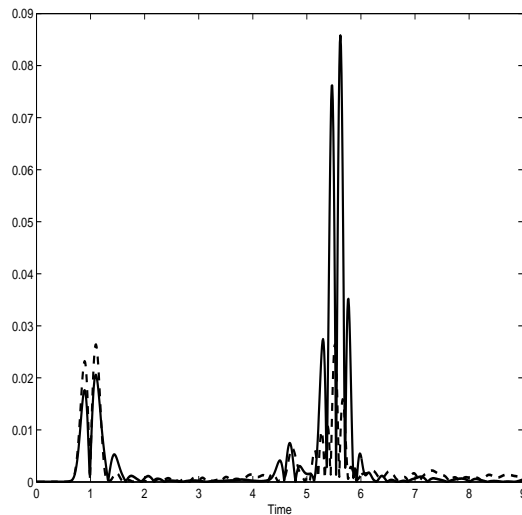

Figure 1: Error curves for the DG solution (dash line) and FD solution (solid line).

Acknowledgements

References

[1] R. BERNARDES, T. SANTOS AND J. CUNHA-VAZ, *Evaluation of Blood-Retinal Barrier Function from Fourier Domain High-Definition Optical Coherence Tomography*, in IFMBE Proceedings 25/XI, 2009, 316–319.

[2] R. BERNARDES, T. SANTOS, P. SERRANHO, C. LOBO, AND J. CUNHA-VAZ, *Noninvasive evaluation of retinal leakage using OCT*, Ophtalmologica **226(2)** (2011) 29–36.

[3] B. BOUMA AND G. TEARNEY, *Handbook of optical coherence tomography*, Marcel Dekker, New York, 2002.

[4] S. DESCOMBES, S. LANTERI AND L. MOYA, *Locally implicit time integration strategies in a discontinuous Galerkin method for Maxwell's equations*, J. Sci. Comput. **56** (2013) 190–218.

[5] J. HESTHAVEN AND T. WARBURTON, *Nodal High-Order Methods on Unstructured Grids: I. Time-Domain Solution of Maxwell's Equations*, J. Comput. Phys. **181** (2002) 186–221.

[6] J. S. HESTHAVEN AND T. WARBURTON, *Nodal Discontinuous Galerkin Methods: Algorithms, Analysis, and Applications*, Springer Verlag, New York, 2008.

[7] L. JUNQUEIRA AND J. CARNEIRO, *Basic Histology: Text & Atlas (Junqueira's Basic Histology)*, McGraw-Hill Medical, 2005.

[8] M. KÖNIG, K. BUSCH AND J. NIEGEMANN, *The Discontinuous Galerkin Time-Domain method for Maxwell's equations with anisotropic materials*, Phot. Nano. Fund. Appl. **8** (2010) 303–309.

[9] C. MÜLLER, *Foundations of the Mathematical Theory of Electromagnetic Waves*, Springer Verlag, Berlim, 1969.

[10] J. NIEGEMANN, R. DIEHL AND K. BUSCH, *Efficient low-storage Runge-Kutta schemes with optimized stability regions*, J. Comput. Phys. **231** (2012) 364–372.

[11] W. REED, T. HILL, *Triangular mesh methods for the neutron transport equation*, Los Alamos Scientific Laboratory. LA-UR-73-479 (1973).

[12] R. N. RIEBEN, G. H. RODRIGUE AND D. A. WHITE, *A high order mixed vector finite element method for solving the time dependent Maxwell equations on unstructured grids*, J. Comput. Phys. **204** (2005) 490–519.

A. Araújo, S. Barbeiro, L. Pinto, R. Bernardes et al.

[13] Z. S. Sacks, D. M. Kingsland, R. Lee and J.-F. Lee, *A perfectly matched anisotropic absorber for use as an absorbing boundary condition*, IEEE Trans. Antennas. Propag. **43** (1995) 1460–1463.

[14] J. M. Schmitt, A. Knüttel, and R. F. Bonner, *Measurement of optical properties of biological tissues by low-coherence reflectometry*, Appl. Opt. **32** (1993) 6032–6042.

[15] P. Serranho, M. Morgado and R. Bernardes *Optical Coherence Tomography: a concept review* In: Optical Coherence Tomography: A Clinical and Technical Update. R. Bernardes & J. Cunha-Vaz Eds., Springer-Verlag, 2012, 139–156

[16] A. Taflove and S. C. Hagness, *Computational Electrodynamic: The Finite-Difference Time-Domain Method (2nd ed.)*, Artech House, Norwood, MA, 2000.

[17] K. S. Yee, *Numerical solution of initial boundary value problems involving maxwell's equations in isotropic media*, IEEE Trans. Antennas. Propag. **14** (1966) 302–307.